A&A 446, 155–170 (2006)
DOI: 10.1051/0004-6361:20052871

Astronomy & Astrophysics

Radio and X-ray variability of young stellar objects in the *Coronet* cluster

J. Forbrich[1,2], Th. Preibisch[1], and K. M. Menten[1]

[1] Max-Planck-Institut für Radioastronomie, Auf dem Hügel 69, 53121 Bonn, Germany
e-mail: forbrich@mpifr-bonn.mpg.de
[2] Astrophysikalisches Institut und Universitäts-Sternwarte Jena, Schillergäßchen 2-3, 07745 Jena, Germany

Received 11 February 2005 / Accepted 7 September 2005

ABSTRACT

The *Coronet* cluster in the nearby R CrA dark cloud offers the rare opportunity to study at least four "class I" protostellar sources as well as one candidate "class 0" source, a Herbig Ae star, and a candidate brown dwarf within a few square arcminutes – most of them detected at radio- *and* X-ray wavelengths. These sources were observed with the Very Large Array (VLA) at λ = 3.5 cm on nine occasions in 1998, spread over nearly four months. The source IRS 5, shown earlier to emit circularly polarized radio emission, was observed to undergo a flux increase accompanied by changes in its polarization properties. Comparison with VLA measurements taken in January 1997 allows analysis of longer-term variability. In addition to this radio monitoring, we analyze archival *Chandra* and XMM-*Newton* X-ray data of these sources. Three class I protostars are bright enough for X-ray spectroscopy, and we perform a variability analysis for these sources, covering a total of 154 ks spread over more than two and a half years. Also in X-rays, IRS 5 shows the most pronounced variability, whilst the other two class I protostars IRS 1 and IRS 2 have more stable emission. X-ray data is also analyzed for the recently identified candidate class 0 source IRS 7E, which shows strong variability as well as for the Herbig Ae star R CrA for which we find extremely hot X-ray–emitting plasma. For IRS 1, 2 and 5, the hydrogen column densities derived from the X-ray spectra are at about half the values derived with near-infrared techniques, a situation similar to what has been observed towards some other young stellar objects.

Key words. stars: pre-main sequence – stars: individual: R CrA – radio continuum: stars – X-rays: stars

1. Introduction

The energetic processes in and around pre-main sequence stars lead to considerable variability over a wide spectral range. The study of radio and X-ray emission allows to probe energetic processes in the coronae of these stars (see Feigelson & Montmerle 1999) in all their evolutionary stages: Low-mass stars evolve through a series of stages termed class 0 to class III (Lada 1987, and e.g. André et al. 2000). In the class 0 stage, gravitational collapse has started, but most of the material is still in the circumstellar envelope. Soon after the onset of accretion, powerful bipolar outflows develop. The luminosity of class I sources is still mainly due to accretion, although a considerable fraction of the final matter has already been accreted. The canonical age of such objects is assumed to be about 10^5 years. The class I phase is followed by the class II (=classical T Tauri star) and class III (=weak-line T Tauri star) phases, during which the circumstellar material plays a consecutively diminishing role in the protostar's evolution.

1.1. X-rays from young stellar objects

X-ray emission from classical and weak-line T Tauri stars has been known for some time and is thought to be produced in magnetically confined plasma in the coronae (Feigelson & Montmerle 1999; Favata & Micela 2003). During the 1990s, X-ray emission towards a few even younger class I protostars was discovered (reviewed by Neuhäuser 1997). With the launches of *Chandra* and XMM-*Newton*, X-ray observatories with higher spatial resolution and better sensitivity to harder photons (which are less affected by extinction) became available, allowing better studies of star-forming regions, such as the Orion Nebula Cluster (Garmire et al. 2000; Feigelson et al. 2002, 2003; Getman et al. 2005), ρ Ophiuchi (Imanishi et al. 2001; Ozawa et al. 2005) or IC 348 (Preibisch & Zinnecker 2001, 2002). However, the processes giving rise to magnetic activity in young stars in general and class 0/I protostars in particular are still poorly understood. For a review of the associated high-energy processes, see Feigelson & Montmerle (1999), Preibisch (2004a), or, in the framework of stellar radio and X-ray astronomy, Güdel (2002, 2004).

Many X-ray emitting class I protostars have X-ray luminosities which are more than ten times higher than those of typical T Tauri stars while their X-ray spectra are harder and show stronger absorption at lower energies due to circumstellar extinction. Powerful flares have been observed frequently (e.g. Imanishi et al. 2001). Until now, however, only relatively few X-ray–detected class I protostars are known. A ROSAT

survey of young stellar objects yielded only eleven class I sources (Carkner et al. 1998). Searching for more X-ray detections among class I protostars yields very different detection rates. While Imanishi et al. (2001), studying the ρ Oph cloud, detect ∼70% of the class I sources in X-rays, a result confirmed by Ozawa et al. (2005), Preibisch (2004b) detects four out of 19 class I sources in the Serpens dark cloud. Imanishi et al. (2001) and Preibisch (2004b) suggest that class I sources might be intrinsically more variable at X-ray wavelengths than protostars in more evolved evolutionary stages, i.e., class II and class III young stellar objects.

The first tentative X-ray detection of two candidate class 0 sources (in OMC-3) was reported by Tsuboi et al. (2001). However, the identification as class 0 sources is ambiguous, Tsujimoto et al. (2004) concluding that in one case the X-ray emission is shock-induced by jets from a nearby class I source. The detection of an X-ray flare from IRS 7E, a candidate class 0 source in the *Coronet* cluster, was first presented by Hamaguchi et al. (2005) and is discussed further in this paper.

When it comes to physical explanations for the hard X-ray emission from class I protostars, often a magnetic interaction of the accretion disk and the stellar magnetosphere is put forward. In the model of Hayashi et al. (1996), closed magnetic loops connecting the central star and the disk are twisted by the rotation of the disk (see also e.g. Shu et al. 1997; Birk et al. 2000; Isobe et al. 2003). The loops expand with increasing twist until reconnection takes place, hot plasma giving rise to the X-ray and, conceivably, nonthermal radio emission. This mechanism predicts flare periodicity on the order of the rotation period of the innermost parts of the disk and is compatible with observed flare durations, i.e. several hours to days (e.g. Koyama et al. 1996). Montmerle et al. (2000), basing their conclusions on the occurence of quasi-periodic flares on YLW 15, propose an evolutionary scenario explaining X-ray properties of protostars as due to their rotation velocity. In this picture, young class I sources in which the rotation of star and disk is not yet synchronous, would constitute the strongest X-ray emitting population of star formation. This phase quickly comes to an end (after a few 10^5 years) and coronal activity becomes the dominant source for X-ray emission. Thus, the following part of the class I stage is already comparable to the class II phase with synchronous rotation, however with much more extinction due to circumstellar material than in the later evolutionary stages. Until now, with no further periodicities found, observational evidence for star-disk magnetic coupling in these objects is inconclusive (Montmerle 2003). However, Favata et al. (2005) find evidence for such coupling from the analysis of intense X-ray flares necessitating large magnetic structures.

1.2. Radio emission from young stellar objects

Thermal as well as nonthermal radio emission has been observed towards pre-main sequence stars. Distinctive features of nonthermal radio emission include rapid variability, circular polarization, negative spectral indices and exceedingly high brightness temperatures (at high spatial resolution). Identified as gyrosynchrotron emission from mildly relativistic electrons gyrating in magnetic fields in this context, nonthermal radio emission is a direct tracer of circumstellar magnetic activity. Thermal radio emission is thought to be produced by ionized material e.g. at the base of outflows. The radio properties of young stellar objects are reviewed by e.g. André (1996); for a discussion of gyrosynchrotron radio emission from a young B star, see André et al. (1988).

A number of X-ray emitting classical and weak-line T Tauri stars are sources of nonthermal radio emission produced in large-scale magnetic structures in the coronae of these objects also giving rise to thermal X-ray emission from coronal plasmae. In particular, circularly polarized radio emission indicative of gyrosynchrotron emission has been observed towards several YSOs (e.g. André et al. 1988, 1992; White et al. 1992; Skinner 1993; Phillips et al. 1993; Rodríguez et al. 1999).

Class I protostars have mostly been observed to be thermal radio sources. Shang et al. (2004) model the centimetric free-free emission of class I protostars based on the X-wind model (Shu et al. 1997) with X-ray emission as the main ionization source, and indeed some of the class I sources showing X-ray emission are known radio sources as well (e.g. Grosso et al. 1997; Feigelson et al. 1998; Smith et al. 1999). However, already at the base of such outflows, the material becomes optically thick so that emission from the immediate surroundings of the star – e.g. nonthermal radiation caused by magnetic fields – can easily be hidden. Gibb (1999) proposes a scenario where only the earliest and latest stages of star formation emit at radio wavelengths: With fading accretion, the (thermal) jet emission decreases while at the same time presumably a stellar magnetic field builds up, giving rise to nonthermal emission. As at X-ray wavelengths, not all class I protostars are detected at radio wavelengths either: Lucas et al. (2000) detect four out of seven class I sources with outflow activity in Taurus, while Lehtinen et al. (2003) detect one out of four associated to Cederblad 110, interestingly the one with the largest far-infrared flux. These low numbers remain inconclusive concerning the fraction of radio-detected class I sources but might still point towards an evolutionary dependence within the class I stage.

Among the three class I sources discussed here in detail, one (IRS 5) is observed to emit nonthermal radio emission (as reported earlier by Feigelson et al. 1998). This source is in fact the only class I protostar known to emit such radiation. Already its circular polarization is a clear sign, additionally its short-term variability is difficult or impossible to reconcile with thermal emission.

At present, little is known about the temporal correlation of the X-ray and radio emission, especially when nonthermal radio emission is concerned. Here, we study these phenomena separately, based on non-simultaneous observations. The only possibility to learn more about these sources consists of simultaneous multi-wavelength studies looking for correlations in the variability at different wavelengths, especially in the radio and X-ray regimes. Until now, only few systematic attempts of such observations of young stellar objects have been made: Feigelson et al. (1994) observed a magnetically active T Tauri star, Guenther et al. (2000) targeted pre-main sequence stars in the Taurus-Auriga region, specifically V773 Tau, and Gagné et al. (2004) observed pre-main sequence stars in the ρ Oph

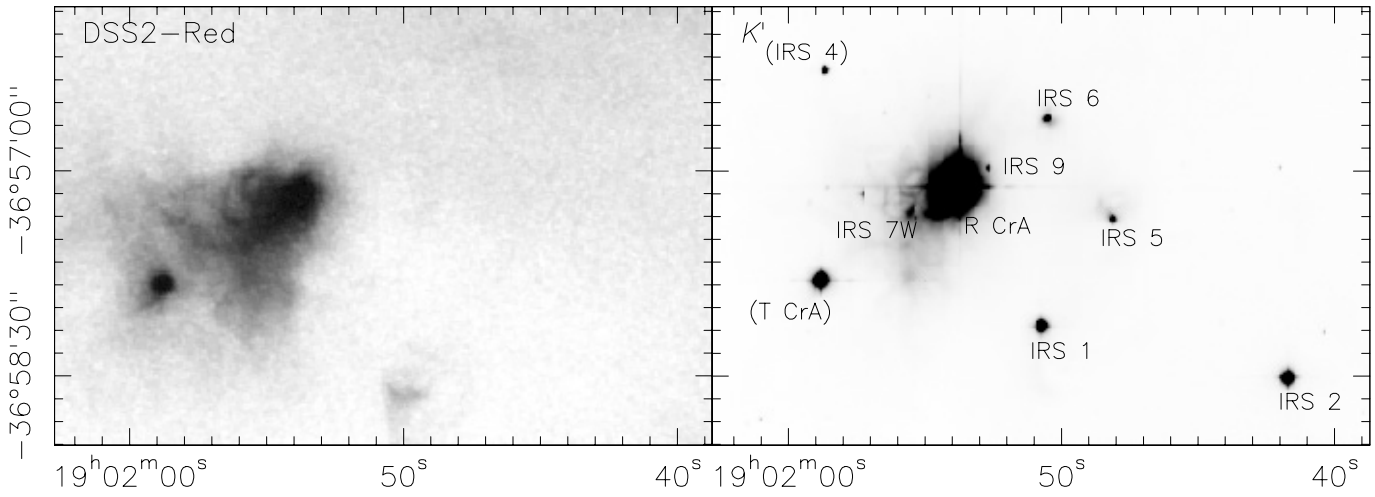

Fig. 1. Optical (DSS2-Red, *left*) and near-infrared (*K′*, *right*) views of the *Coronet* cluster. T CrA, seen at left, is not covered by the radio data presented here. It is marginally detected in X-rays (Skinner et al. 2004). The *K′* image is from Hodapp (1994), coordinates are J2000.

cloud complex. However, only in the latter case two class I protostars were targeted but not detected at both radio and X-ray wavelengths. Simultaneous observations like these can be very valuable, as underlined by the serendipitous discovery of an enormous flare at radio and X-ray wavelengths, apparently from a highly obscured weak-line T Tauri star in Orion (Bower et al. 2003).

1.3. Protostars in the Coronet cluster

The Corona Australis (CrA) molecular cloud complex is a nearby region with ongoing star formation, at a distance of only 150 pc, which is similar to that of the Taurus and ρ Oph dark cloud complexes (Finkenzeller & Mundt 1984)[1]. Taylor & Storey (1984) found a compact cluster of infrared sources in the densest part of the cloud complex close to the Herbig Ae star R CrA, calling it the *Coronet* cluster. Figure 1 shows the DSS2-Red and *K′*-band views of its central region, clearly showing a number of deeply embedded sources.

The *Coronet* cluster is an association of young stellar objects mostly identified at radio as well as X-ray wavelengths. It is comprised of at least five deeply embedded class I protostars (Wilking et al. 1986, 1992, 1997), four of which are covered by the observations presented here[2]. Koyama et al. (1996) reported the detection of hard X-ray emission towards these five protostars. Three of these sources could be verified at higher angular resolution by ROSAT (Neuhäuser & Preibisch 1997), more ROSAT-detected young stellar objects were reported by Neuhäuser et al. (2000). First results from *Chandra*-ACIS observations of this region were presented by Garmire & Garmire (2003) who detected more than 70 sources in a 20 ks exposure.

The *Coronet* cluster has been analyzed at radio wavelengths already several times. Brown (1987) carried out VLA observations at $\lambda = 6$ cm in 1985, identifying five sources associated with young stellar objects. Suters et al. (1996) analyze the radio variability of pre-main-sequence stars using archival VLA (1985-1987) and Australia Telescope (1992) data, while Feigelson et al. (1998) report on VLA observations at 3.5 cm, taken in 1997. They detect circular polarization toward the class I protostar IRS 5.

Studying dust emission from the region at $\lambda = 1.2$ mm, Chini et al. (2003) report several peaks, with the brightest one (called MMS 13 and already detected by Henning et al. 1994) in the vicinity of IRS 7 in the *Coronet* cluster. Millimeter emission is associated with IRS 1, 2 and 5 as well. They conclude that the MMS 13 peak probably is a class 0 source not related to any of the sources observed at other wavelengths. Based on millimeter continuum and molecular line data, Groppi et al. (2004) reached a similar conclusion. Nutter et al. (2005) present higher-resolution submillimeter continuum data resolving MMS 13 into two protostellar and one prestellar source where gravitational collapse has not yet started. This prestellar source is at the position of the class 0 source surmised earlier and is estimated to have a mass of 6 to 11 $M_\odot$, while the envelopes of the protostars considered in this work all have sub-solar mass dust masses. The two protostellar sources are associated with unresolved radio and X-ray sources.

Using near-infrared spectroscopy, Nisini et al. (2005) constrain the accretion rates and evolutionary stages of some *Coronet* protostars. They conclude that IRS 1 and IRS 2 appear to be mostly accretion-powered (accounting for 80% to 65% of $L_{\rm bol}$, respectively), while IRS 5 – a binary source – appears to be a deeply embedded, more evolved object with accretion accounting for only 20% of the bolometric luminosity of one of the components, IRS 5a. IRS 3 and IRS 6a show no signs of accretion. Comparing their derived stellar luminosities and effective temperatures to different models of pre-main sequence evolution, IRS 1 emerges as the youngest object with an age of about 10^5 years, while IRS 2, 5a and 6a apparently have about the same age, closer to 10^6 years in spite of their different accretion properties.

[1] Literature values for the distance range from 130 pc (Marraco & Rydgren 1981) to 170 pc (Knude & Høg 1998).

[2] The fifth one, IRS 3, is located outside the VLA primary beam area and remains undetected at X-ray energies (cf. Nisini et al. 2005).

Table 1. VLA *Coronet* observation dates.

Epoch	Day	Date	IAT interval	Duration	rms (μJy)
R1	1	1998 Jun. 27	07:21:30–08:50:20	01:28:50	30
R2	23	1998 Jul. 19	05:27:10–06:54:00	01:26:50	33
R3	73	1998 Sep. 07	03:08:30–04:07:21	00:58:51	36
R4	85	1998 Sep. 19	01:23:00–03:17:40	01:54:40	24
R5	93	1998 Sep. 27	01:51:40–03:46:10	01:54:30	25
R6	98	1998 Oct. 02	00:03:00–01:56:40	01:53:40	27
R7	102	1998 Oct. 06	00:15:11–01:13:10	00:57:59	36
R8	106	1998 Oct. 10	23:52:50–01:51:10(+1)	01:58:20	23
R9	109	1998 Oct. 13	23:14:40–01:09:30(+1)	01:54:50	25

All epochs except for R1 (BnA) were observed with the B array. Datasets R4-R6 and R8-R9 are from project AM596. Datasets R1-R3 and R7 are from project AK469.

Table 2. Archival X-ray data used in this study.

	Satellite	Obs.	ID	Date	Time (UT)	Duration (s)	Pointing center RA/Dec (J2000)
1	*Chandra*	19	C1	2000 Oct. 07	17:01:59–23:11:01	19958	19 01 50.6 –36 57 30.0
2	XMM-*Newton*	0111120101	X1	2001 Apr. 09	09:32:16–15:56:46	26445	19 01 49.4 –36 55 41.4
3	XMM-*Newton*	0146390101	X2	2003 Mar. 28	08:50:45–18:32:49	36715	19 01 37.2 –36 51 02.3
4	XMM-*Newton*	0146390201	X3	2003 Mar. 29	19:35:00–04:00:38(+1)	32211	19 01 37.2 –36 51 02.5
5	*Chandra*	3499	C2	2003 Jun. 26	12:58:10–00:16:08(+1)	38126	19 01 50.6 –36 57 30.0

2. Observations and data analysis

2.1. Radio observations

Here we present the results of a radio monitoring campaign at $\nu = 8.44$ GHz of the *Coronet* cluster, carried out with the NRAO Very Large Array (VLA) between 1998 September 19 and October 13. The sources, which are all within the 5.4 arcmin FWHM primary beam, were observed five times, separated by a few days each. Originally, these observations were scheduled to be simultaneous with X-ray monitoring, but ROSAT unexpectedly went out of operation before the campaign was to begin. The VLA was observing in the B configuration (program ID AM596) at $\nu = 8.44$ GHz with two intermediate frequency (IF) pairs, offset by each IF band's width, 50 MHz. One IF of each pair detected right circular polarization (RCP), the other one left circular polarization (LCP). The phase center was $(\alpha, \delta)_{\rm J2000} = 19^{\rm h}01^{\rm m}48^{\rm s}, -36°57'59''$. These data are complemented by four additional epochs in 1998, also taken with the VLA in B/BnA configuration (program ID AK469) at $\nu = 8.44$ GHz, increasing the total to nine epochs, now starting on June 27, 1998. The source coverage is slightly different due to a different phase center, $(\alpha, \delta)_{\rm J2000} = 19^{\rm h}01^{\rm m}55.6^{\rm s}, -36°57'09.6''$. Details on the dates and durations of the different observation epochs are given in Table 1. These data can be compared with measurements taken by Feigelson et al. (1998) on 1997 January 19 and 20 (see Table 4).

The VLA data were analyzed using NRAO's Astronomical Image Processing System (AIPS). An absolute flux density scale was established by observations of 3C286, the nearby phase calibrator 1924−292 was observed every ten minutes. At a declination of nearly −37°, the *Coronet* cluster is observable with the VLA only at very low elevations (<18°), increasing problems with phase instabilities caused by the atmosphere. Here, however, by using self-calibration, these effects could be minimized. All observation epochs were phase-only self-calibrated, as the low flux densities did not warrant self-calibration of, both, phases plus amplitudes. Following this, Stokes-I and Stokes-V were imaged separately, with the input *uv*-data split into different time intervals. The polarization of the secondary calibrator 1924−292 is $\lesssim$1%. Source positions and fluxes were determined, using the AIPS task SAD, by fitting Gaussians to each detection. The light curves thus derived are shown in Fig. 3. The root mean square (rms) noise level in the Stokes I and V maps for the different epochs is shown in Table 1. For the detection of weak sources, the five AM596 observations were combined, yielding a map with an rms of <12 μJy. The synthesized beam size for this combined data is $1.93 \times 0.63''$ at position angle $-0.51°$.

2.2. Archival X-ray data

In addition to the radio data, we studied archival X-ray data of the *Coronet* sources. On 2000 October 7, this region was observed with *Chandra*, using the Advanced CCD Imaging Spectrometer in its imaging mode ACIS-I in order to search for X-rays from young stars in a 20 ks exposure (Garmire & Garmire 2003). A second ACIS-I observation of this region, with a 38 ksec exposure, was carried out on 2003 June 26. Additionally, there have been three XMM-*Newton* observations of the *Coronet* region: on 2001 April 9 there was a 26 ks exposure and on 2003 March 28/29 two consecutive observations of 36 ks and 32 ks were carried out. While the first XMM-*Newton* observation was taken through the "thin" filter, the "medium" filter was used for the latter two observations. Details on the X-ray data analyzed here are listed in Table 2. Our analysis of the archival X-ray data focuses on the three X-ray brightest

sources among the sample discussed here, IRS 1, 2 and 5 because they are bright enough for a spectral analysis. These three sources are class I protostars.

Chandra X-ray data were analyzed using the Chandra Interactive Analysis of Observations (CIAO) 3.1 software package together with CALDB 2.28. Apertures used were three or five (IRS 1, 2, and 5) arcseconds in diameter. Spectra were prepared with the task *psextract*, including the creation of response matrices and ancillary response files. Finally, spectra bin sizes were determined by a minimum event number per bin of fifteen.

XMM-*Newton* data were analyzed using the Science Analysis System (SAS) 6.0.0. Due to the superior signal-to-noise ratio among XMM imaging instruments, we only make use of the EPIC-PN data here. We generally used apertures with a diameter of 32″, but in cases of close neighbouring sources, we defined smaller (14″ diameter) non-overlapping extraction regions. These apertures encircle approximately 66% and 40% of the point source flux[3], so that corresponding correction factors had to be taken into account in the luminosity determination. Spectroscopy involved the creation of response matrices and ancillary response files using the tasks *rmfgen* and *arfgen*, respectively. Finally, the spectra were binned with the same minimum event number criterion as was used for the *Chandra* data.

Models were fitted to all background-subtracted spectra with *Sherpa* from the CIAO 3.1 software package, using Monte Carlo multi-parameter fits. The spectral model consists of the Astrophysical Plasma Emission Code (APEC) with an absorption factor. This code calculates the emission spectrum from collisionally ionized diffuse gas. The main fit parameters are the plasma temperature, the absorbing hydrogen column density and the element abundances compared to solar values.

After a determination of elemental abundances from the Fe K line at 6.7 keV from one spectrum per source, an absorbed APEC emission model was fitted to the spectra. It turned out that the spectra can be well described with a single-temperature model; there was no need to assume two temperature components. However, due to the high absorbing column densities toward the sources, softer emission components might easily be extincted. The uncertainties of the best-fit parameter values were estimated with the *Sherpa* task "uncertainty". Based on these fits, the count rates in the lightcurves were converted into unabsorbed flux using the PIMMS software (Mukai 1993) and finally, into luminosity units (energy range 0.5–10 keV), assuming a distance of $d = 150$ pc.

3. Results

After a general discussion of the 1998 VLA monitoring and the analysis of archival X-ray data, individual source properties will be summarized.

[3] As given in the XMM-*Newton* User's Handbook V2.2.

3.1. Radio monitoring

In Stokes-*I*, eight sources can be detected throughout all five AM596 observation epochs, taking a 5σ detection limit as the criterion for source existence. These sources are also detected throughout the AK469 data with the exception of IRS 2, not detected due to primary beam attenuation far from the observation's phase center. An image created from the combined AM596 *uv* data is shown in Fig. 2. Five weak additional sources only emerge from this integration of the five AM596 observation epochs, including the T Tauri star IRS 6. In Stokes-*V* only IRS 5 was detected, showing epoch-averaged circular polarization degrees between 0% and 23%. IRS 5 at the same time is the most spectacularly variable source in this dataset: Starting at a relatively high emission level, but interestingly without detected circular polarization, the source dims, then rises sharply towards two peaks at the end of the period covered, accompanied by changes in its polarization. Analyzing the data in shorter intervals, the Stokes-*V* emission of IRS 5 remains variable at timescales of 0.5 h while this is not the case for any of the sources in Stokes-*I*. The remaining sources show diverse degrees of variability, but to a lesser extent (Fig. 3). All sources detected in single epochs have been detected at radio wavelengths before. The source fluxes derived from the VLA observations are summarized in Table 4, together with the 3.5 cm fluxes from Feigelson et al. (1998) for comparison.

3.2. Archival X-ray data

At X-ray wavelengths, nine sources are clearly detected, including an unidentified weak source (No. 3) only detected by *Chandra* (see Tables 3 and 5). Figure 2 shows the combined *Chandra* data, with the combined XMM-*Newton* data shown as an inset. It is interesting to compare this X-ray view with the radio view in Fig. 2. The five weak radio sources only emerging in the complete VLA data all remain undetected in X-rays together with the Radio Sources 5 and 9 (Brown 1987). However, the class I protostar IRS 9 – clearly detected in X-rays, even with a flare in the C1 observation – remains undetected at radio wavelengths, together with the weak X-ray source No. 3 not showing any counterpart at other wavelengths. Comparing the count rates for these sources derived from the five X-ray datasets shows that there is considerable variability in many cases (Table 5). For the three class I protostars IRS 1, 2 and 5, this is corroborated by the luminosity curves (Fig. 7) and the corresponding spectra (Fig. 5). All three sources have X-ray luminosities on the order of several 10^{30} erg/s. IRS 5 emerges again as the most variable source.

The elemental abundances for the three sources, as derived from the 6.7 keV Fe K line emission, are 0.5 ± 0.2 (IRS1, X1), 0.7 ± 0.1 (IRS2, X3) and 0.26 ± 0.05 (IRS5, X3) relative to solar abundances. There is no evidence for fluorescent emission of weakly ionized or neutral iron at energies below 6.7 keV. Fitting absorbed APEC emission models to the spectra leads to the results depicted in Fig. 6 and listed in Table 6. All three sources show high absorbing column densities (several 10^{22} cm^{-2}) and hot plasma emission (several 10^7 K). There are signs of long-term variability in the absorbing column

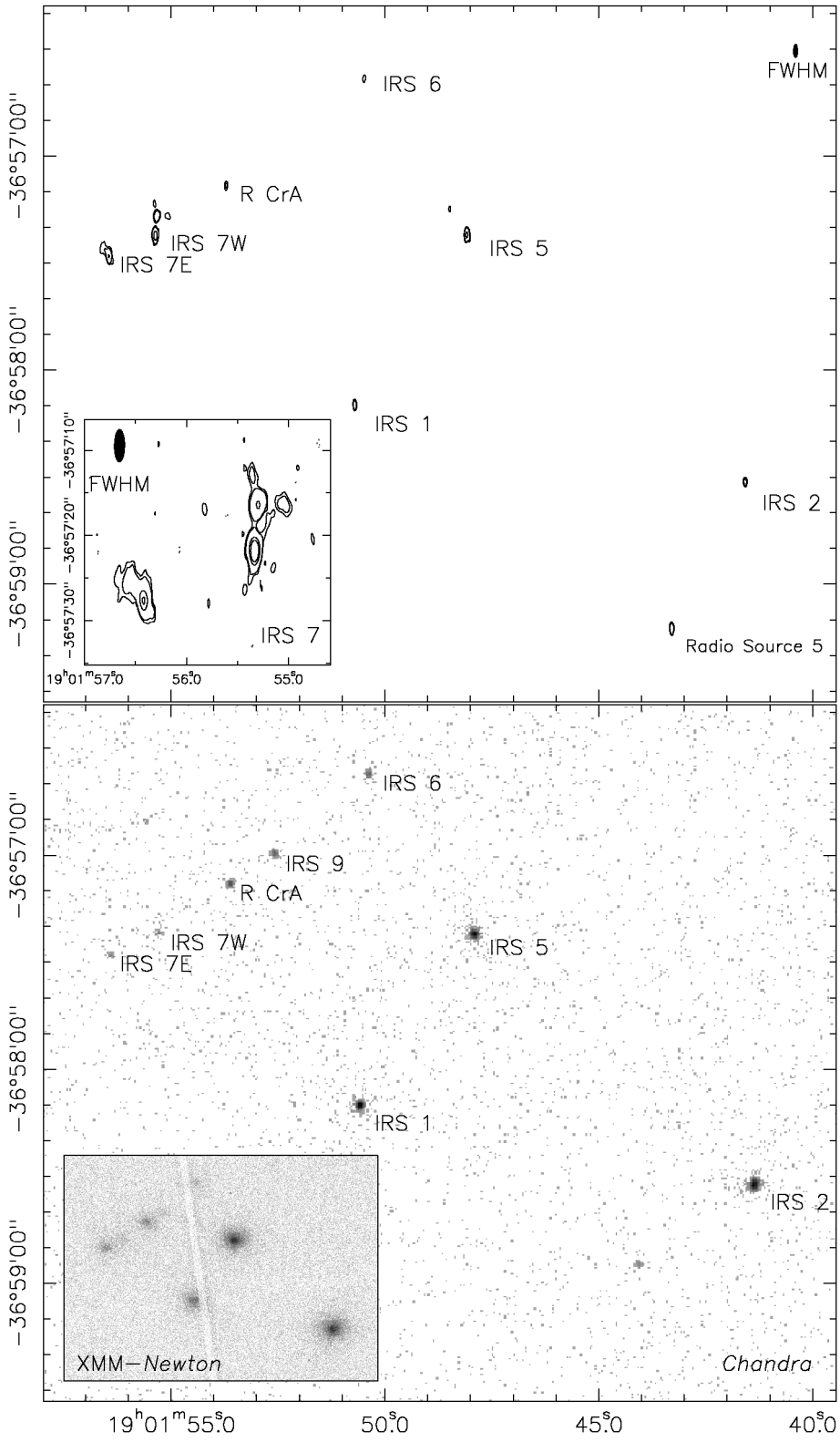

Fig. 2. *Upper panel*: image made from the combined *uv* data of all five VLA observation epochs. Contours shown are 5, 10 and 100σ in the main plot and –3 (dashed), 3, 5, 50 and 100σ in the inset showing IRS 7. Coordinates are J2000.0. *Lower panel*: the same view, showing the merged *Chandra* ACIS-I data. The inset shows approximately the same view in the merged XMM-*Newton* data (MOS+EPN, X1-X3).

densities, especially towards IRS 2 and IRS 1. Note that the X2 and X3 observations are consecutive while a total range of about 2.5 years is covered. Tentatively, there is a trend for the emission being harder when the sources are brighter, although the situation is inconclusive.

Interestingly, though, the hydrogen column densities as derived from the X-ray spectra for IRS 1, 2, and 5 are at around half the values derived by Nisini et al. (2005) from near-infrared colours[4] (see Table 7). In order to check the significance of this discrepancy, we tried to fit the spectra while freezing the absorbing column density $N_{\rm H}$ to the value derived from NIR colours. This lead to very poor fits (large χ^2) in all cases,

[4] Adopting $A_{\rm V} = 15.9 \cdot E(H-K)$ (Rieke & Lebofsky 1985).

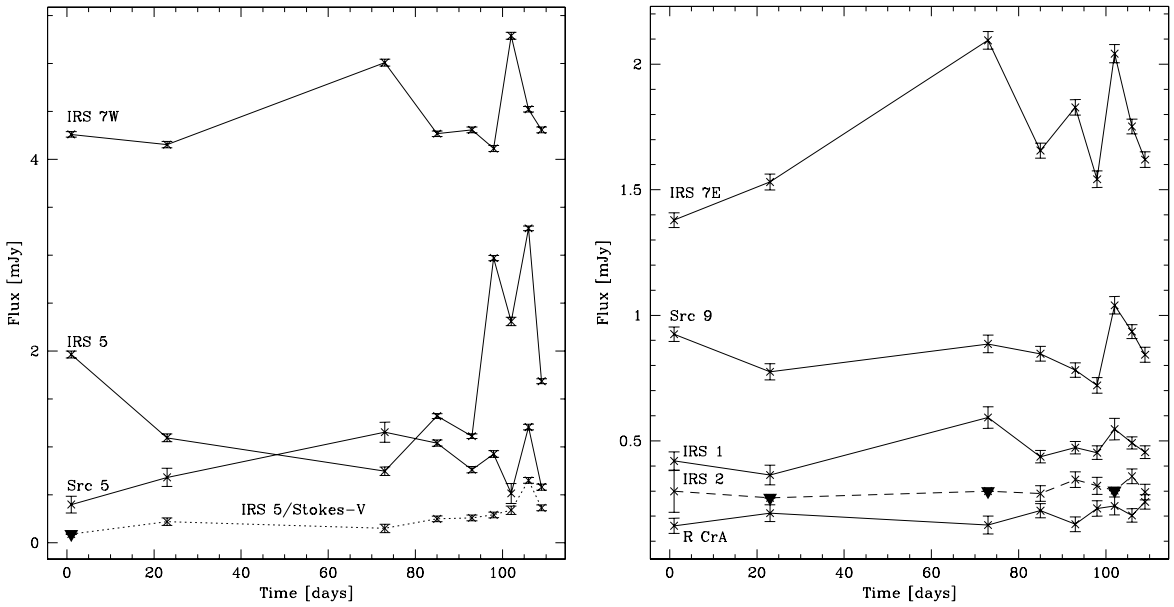

Fig. 3. Radio flux curves of sources identified in the 1998 VLA data. Error bars indicate the uncertainty estimates given by the AIPS task "sad", they are based on actual noise (1σ) rather than the quality of the fit. Filled triangles denote upper limits. Also shown is Stokes-*V* for IRS 5.

Table 3. Positions and identification of *Coronet* radio and X-ray sources.

No.	Position (J2000.0)	Source ID[a]
1	19 01 41.6 –36 58 31	IRS 2 (I)
2	19 01 43.3 –36 59 12	Source 5[b]
3	19 01 44.2 –36 58 54	
4	19 01 48.1 –36 57 22	IRS 5 (I)
5	19 01 48.5 –36 57 15	
6	19 01 50.5 –36 56 38	IRS 6 (T)
7	19 01 50.7 –36 58 09	IRS 1 (I)
8	19 01 52.6 –36 57 01	IRS 9 (I)
9	19 01 53.7 –36 57 08	R CrA (H)
10	19 01 55.0 –36 57 16	
11	19 01 55.3 –36 57 16	Source 9[b]
12	19 01 55.3 –36 57 22	IRS 7W
13	19 01 55.4 –36 57 13	
14	19 01 56.4 –36 57 28	IRS 7E (0?)
15	19 01 56.5 –36 57 26	

[a] Types: (0) = class 0, (I) = class I, (T) = T Tau, (H) = HAe.
[b] As defined by Brown (1987).

demonstrating that the large $N_{\rm H}$ values are inconsistent with the X-ray spectra. Additionally, by using a Monte Carlo fitting scheme, the parameter space was checked for multiple minima, but again no acceptable model was found for large $N_{\rm H}$ values. The empirical relation is $N_{\rm H}[{\rm cm}^{-2}] \approx 2 \times 10^{21} \times A_{\rm V}[{\rm mag}]$ (Ryter 1996; Vuong et al. 2003). A similar discrepancy has been observed previously towards the young stellar objects L1551 IRS 5 (Bally et al. 2003), EC 95 (Preibisch 2003a), and towards SVS 16 (Preibisch 2003b). Possible solutions to this "extinction problem" are configurations in which the protostar and its X-ray emission become detached, so that the absorbing column densities for the infrared and X-ray emission become different. Scenarios include X-ray emission from jet shocks close to the protostar, X-rays scattered towards the observer by circumstellar material, and huge coronal structures.

For six of the young stellar objects studied here, it is possible to reliably determine X-ray luminosities based on their spectra. The radio and X-ray luminosities of these sources have been plotted into Fig. 8 together with an empirical relationship for active late-type stars from Benz & Guedel (1994). The underlying physics of this relation is that the acceleration of synchrotron-emitting electrons and the heating of the coronal plasma leading to X-ray emission are accomplished by the same mechanisms. The *Coronet* YSOs appear to be compatible with this relationship.

Comparing the X-ray luminosities to the bolometric luminosities (see Table 8), it turns out that IRS 2, 5, 1, and R CrA are all in the unsaturated regime $L_{\rm X}/L_{\rm bol} < 10^{-3}$ (Fleming et al. 1995), but a lot more active than the sun ($(L_{\rm X}/L_{\rm bol})_\odot \approx 10^{-6}$), IRS 5 being the most active source with a ratio of $\log(L_{\rm X}/L_{\rm bol}) = -3.4$.

3.3. Synthesis

3.3.1. The class I protostars IRS 2, IRS 5, IRS 1, and IRS 9

IRS 2 does not show significant radio variability in any time interval covered by our observations (Fig. 3 and Table 4). The flux is, however, at about half the value determined by Feigelson et al. (1998). IRS 2 is one of the strongest X-ray sources among the objects studied here. The overall count rate in the C1 *Chandra* observation is twice as high as during the C2 observation which is clearly visible in the luminosity curves (Fig. 7). The XMM-*Newton* count rates are less diverse. Variability is seen also within observations, especially X1, showing a continuous increase, and X3, showing a sudden increase in the second half of the observation.

Table 4. *Coronet* sources, radio data.

No.	R1 (mJy)	R2 (mJy)	R3 (mJy)	R4 (mJy)	R5 (mJy)	R6 (mJy)	R7 (mJy)	R8 (mJy)	R9 (mJy)	Combined[a] (mJy)	FCW98[b] (mJy)
1	0.30	<0.27[c]	<0.30[c]	0.29	0.35	0.32	<0.30[c]	0.36	0.30	–	0.67
2	0.40	0.68	1.15	1.04	0.76	0.93	0.52	1.21	0.58	–	1.08
3	n.d.	n.d.	n.d.	n.d.	n.d.	n.d.	n.d.	n.d.	n.d.	–	n.d.
4	1.96	1.10	0.75	1.32	1.11	2.97	2.31	3.28	1.67	–	1.36
4*V*	<0.09[c]	0.22	0.15	0.25	0.26	0.29	0.34	0.65	0.36	–	0.23
5	n.d.	n.d.	n.d.	n.d.	n.d.	n.d.	n.d.	n.d.	n.d.	0.10	n.d.
6	n.d.	n.d.	n.d.	n.d.	n.d.	n.d.	n.d.	n.d.	n.d.	0.15	n.d.
7	0.42	0.36	0.59	0.44	0.47	0.45	0.55	0.49	0.46	–	0.45
8	n.d.	n.d.	n.d.	n.d.	n.d.	n.d.	n.d.	n.d.	n.d.	<0.035[c]	n.d.
9	0.16	0.21	0.17	0.22	0.17	0.23	0.24	0.20	0.26	–	0.23
10	n.d.	n.d.	n.d.	n.d.	n.d.	n.d.	n.d.	n.d.	n.d.	0.12	n.d.
11	0.93	0.78	0.89	0.85	0.78	0.72	1.04	0.94	0.84	–	1.58
12	4.26	4.15	5.01	4.27	4.31	4.11	5.29	4.52	4.31	–	3.74
13	n.d.	n.d.	n.d.	n.d.	n.d.	n.d.	n.d.	n.d.	n.d.	0.11	n.d.
14	1.38	1.53	2.10	1.66	1.83	1.54	2.04	1.75	1.62	–	2.03
15	n.d.	n.d.	n.d.	n.d.	n.d.	n.d.	n.d.	n.d.	n.d.	0.13	n.d.

[a] Sources detected in combined AM596 data (10 h).
[b] 3.5 cm flux on 19/20 Jan 1997, as published by Feigelson et al. (1998).
[c] Local 3σ limit, in the case of IRS 2: accounting for primary beam attenuation.

Table 5. *Coronet* sources, X-ray-data.

No.	Source ID	C1[a] (cnts/ks)	C2[a] (cnts/ks)	X1[a] (cnts/ks)	X2[a] (cnts/ks)	X3[a] (cnts/ks)
1	IRS 2	48.7 ± 1.6	26.6 ± 0.9	42.1 ± 1.5	49.4 ± 1.4	54.4 ± 1.5
2	Source 5	n.d.	n.d.	n.d.	n.d.	n.d.
3		0.5 ± 0.2	0.8 ± 0.2	n.d.	n.d.	n.d.
4	IRS 5	13.2 ± 0.9	31.0 ± 0.9	46.5 ± 1.6	40.3 ± 1.3	75.6 ± 1.7
5		n.d.	n.d.	n.d.	n.d.	n.d.
6	IRS 6	2.4 ± 0.4	1.5 ± 0.2	3.4 ± 0.8	0.9[c] ± 0.5	0.5[c] ± 0.5
7	IRS 1	22.9 ± 1.1	30.9 ± 0.9	31.7 ± 1.4	10.9[c] ± 0.7	18.3[c] ± 0.9
8	IRS 9	2.9[b] ± 0.4	2.1 ± 0.3	1.3[d] ± 0.4	2.8[d] ± 0.4	1.2[d] ± 0.4
9	R CrA	3.2 ± 0.5	3.1 ± 0.3	5.2[d] ± 0.6	9.3[d] ± 0.6	6.8[d] ± 0.6
10		n.d.	n.d.	n.d.	n.d.	n.d.
11	Source 9	n.d.	n.d.	n.d.	n.d.	n.d.
12	IRS 7W	0.6 ± 0.2	0.6 ± 0.2	2.1[d] ± 0.4	2.6[d] ± 0.4	4.7[d] ± 0.5
13		n.d.	n.d.	n.d.	n.d.	n.d.
14	IRS 7E	1.0 ± 0.3	0.3 ± 0.1	1.6[d] ± 0.4	3.7[d] ± 0.4	14.7[d] ± 0.8
15		n.d.	n.d.	n.d.	n.d.	n.d.

[a] Background-subtracted count rates (0.5–10 keV) from X-ray datasets as listed in Table 2, *Chandra* and XMM-*Newton* count rates are not directly comparable. Additionally, different filters were used in the XMM-*Newton* observations: "thin" for X1 and "medium" for X2/X3.
[b] Flare.
[c] Source partly covered by chip gap, loss estimated to be ≈20%.
[d] Contamination from neighbouring source.

Already the ROSAT data presented by Neuhäuser & Preibisch (1997) show variability on timescales of months. The X-ray spectra (Fig. 5), can be explained as the emission of hot plasma ($T \approx 4 \times 10^7$ K), absorbed by a column density of $N_{\rm H} \approx 2 \times 10^{22}$ cm^{-2}. Apparently, the absorbing column density towards IRS 2 has continuously diminished over two and a half years, the 3σ errorbars of the first and the last measurements are clearly separated (Fig. 6 and Table 6). This could be caused by a clumpy circumstellar medium, probably involving the circumstellar disk. Nisini et al. (2005) find that accretion accounts for 60% of this object's bolometric luminosity.

IRS 5 shows several flares in our VLA dataset (Figs. 3 and 4, Table 4) and has been observed flaring already once before at 4.9 GHz (Suters et al. 1996). In our data, the source starts at a relatively high flux, dims, and then sharply rises towards two peaks, separated by about nine days. This source

Table 6. X-ray spectral fitting results for IRS 2, 1, 5, and R CrA: Absorbing column density and plasma temperature, with 1σ error margins.

	IRS 2		IRS 5		IRS 1		R CrA	
	$N_{\rm H}$	T	$N_{\rm H}$	T	$N_{\rm H}$	T	$N_{\rm H}$	T
	[10^{22} cm^{-2}]	[MK]	[10^{22} cm^{-2}]	[MK]	[10^{22} cm^{-2}]	[MK]	[10^{22} cm^{-2}]	[MK]
C1	$2.43^{+0.11}_{-0.10}$	$45.9^{+3.3}_{-3.3}$	$3.02^{+0.25}_{-0.22}$	$26.7^{+2.5}_{-2.3}$	$3.75^{+0.31}_{-0.27}$	$63.1^{+9.2}_{-6.6}$	–	–
X1	$1.99^{+0.09}_{-0.08}$	$27.6^{+1.7}_{-1.7}$	$3.50^{+0.15}_{-0.13}$	$30.2^{+1.2}_{-1.2}$	$4.60^{+0.23}_{-0.21}$	$28.7^{+1.4}_{-1.4}$	$1.2^{+0.4}_{-0.3}$	106^{+209}_{-43}
X2	$1.76^{+0.06}_{-0.06}$	$28.8^{+1.4}_{-1.4}$	$4.80^{+0.17}_{-0.15}$	$26.1^{+0.9}_{-0.9}$	$3.21^{+0.31}_{-0.26}$	$48.9^{+7.7}_{-6.0}$	$1.4^{+0.2}_{-0.2}$	100^{+57}_{-26}
X3	$1.60^{+0.15}_{-0.16}$	$36.5^{+5.7}_{-4.2}$	$4.23^{+0.13}_{-0.12}$	$36.8^{+1.1}_{-1.1}$	$2.75^{+0.21}_{-0.18}$	$44.6^{+4.4}_{-4.3}$	1.3[a]	110^{+145}_{-45}
C2	$1.53^{+0.07}_{-0.07}$	$37.5^{+2.7}_{-2.6}$	$4.07^{+0.16}_{-0.14}$	$33.3^{+1.4}_{-1.4}$	$2.36^{+0.09}_{-0.09}$	$32.6^{+1.7}_{-1.6}$	–	–

[a] Frozen parameter, otherwise $N_{\rm H} = 2.6^{+0.5}_{-0.4} \times 10^{22}$ cm^{-2}, $T = 50^{+14}_{-9}$ MK; however this change appears unlikely since X3 is immediately following X2.

Table 7. Comparison of column densities towards IRS 2, 5, and 1 derived from NIR and X-ray emission.

Source	$N_{\rm H}$(NIR)[a] [10^{22} cm^{-2}]	$N_{\rm H}$(X-ray) [10^{22} cm^{-2}]
IRS 2	4.0 ± 0.6	1.9 ± 0.4
IRS 5	9.0 ± 0.6	3.9 ± 0.7
IRS 1	6.0 ± 0.6	3.3 ± 0.9

[a] $A_{\rm V}$ (from Nisini et al. 2005) converted into $N_{\rm H}$ using $N_{\rm H}[{\rm cm}^{-2}] \approx 2 \times 10^{21} \times A_{\rm V}$[mag], see text.

Table 8. Bolometric and X-ray luminosities (derived from X-ray spectra).

Source	$L^a_{\rm bol}$ $L_\odot$	$L_{\rm X}$ 10^{-3} $L_\odot$	$\log(L_{\rm X}/L_{\rm bol})$
IRS 2	16	0.93	−4.2
IRS 5	4	1.70	−3.4
IRS 1	19	0.75	−4.4
R CrA	132	0.18	−5.9

[a] Scaled to $d = 150$ pc from Wilking et al. (1992), for R CrA directly from Lorenzetti et al. (1999).

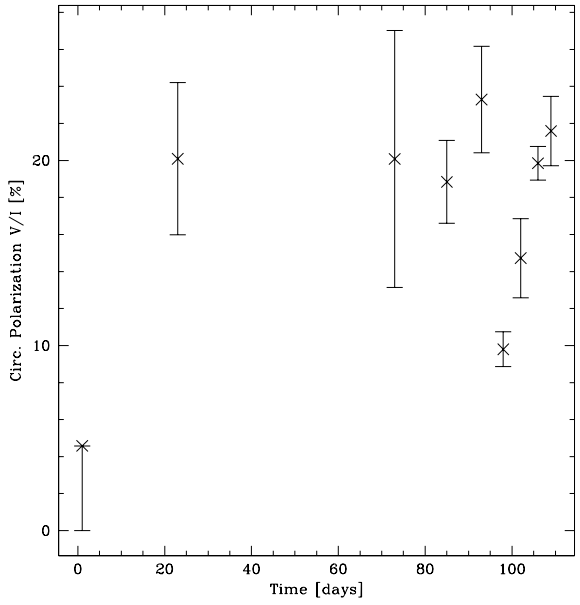

Fig. 4. IRS 5 epoch-averaged polarization degrees in percent. Errors are propagated from those shown in Fig. 3.

was previously reported to emit nonthermal radio emission (Feigelson et al. 1998). Interestingly, the initial high flux of IRS 5 is accompanied by undetectable Stokes-*V* emission. Also when looking at the double peak towards the end of the period covered here, the Stokes-*V* flux appears to be largely uncorrelated to the Stokes-*I* flux: only in the second peak there is a rise in Stokes-*V* flux. Possibly this different behaviour is at least partly due to an averaging effect, given the faster variability in Stokes-*V*: contrary to the Stokes-*I* emission, Stokes-*V* in our data is variable down to timescales of 0.5h, a clear sign of nonthermal emission. In the epoch with the highest Stokes-*V* flux (R8), for example, Stokes-*V* emission was only detected in the first quarter. Two epochs earlier, at the sharp rise in Stokes-*I*, the polarization degree drops from 23% to 10% because only the Stokes-*I* emission increases. In the subsequent epoch, the polarization degree is back at 20% while the total flux increased even further. Feigelson et al. (1998) reported a polarization degree changing between 10% to 37% during a day.

In X-rays, IRS 5 is the most variable object when compared to IRS 1 and IRS 2, within our datasets as well as on longer time scales. The overall count rate in 2003 (C2) is nearly three times as high as in 2000 (C1). In the two consecutive observations X2 and X3, the X3 count rate is nearly twice as high as the X2 count rate. The X3 luminosity curve (Fig. 7) starts with an increase followed by a slight diminution in emission towards the end of the observation. The high-luminosity points at the beginning of the X2 luminosity curve remain unexplained. The X-ray spectra (Fig. 5) show signs of high absorption ($N_{\rm H} \approx 4 \times 10^{22}$ cm^{-2}), the temperature of the emitting plasma is at around $T \approx 3 \times 10^7$ K. There appears to be no significant temporal evolution in these fit parameters (Fig. 6 and Table 6). Nisini et al. (2005) confirm earlier observations by Chen & Graham (1993), finding that IRS 5 is a binary object with only 90 AU separation (scaled to $d = 150$ pc). Thus, the attribution of X-rays to any of the components, or both is difficult. For IRS 5a, they find that accretion accounts for below 20% of the object's bolometric luminosity. While this suggests a deeply embedded object in a later evolutionary stage, Nisini et al. (2005), using standard evolutionary tracks, conclude that IRS 5a has about the same age as IRS 2 ($\approx 5 \times 10^5$–10^6 yr). Already Feigelson & Montmerle (1999) note that the radio properties of this source rather resemble a

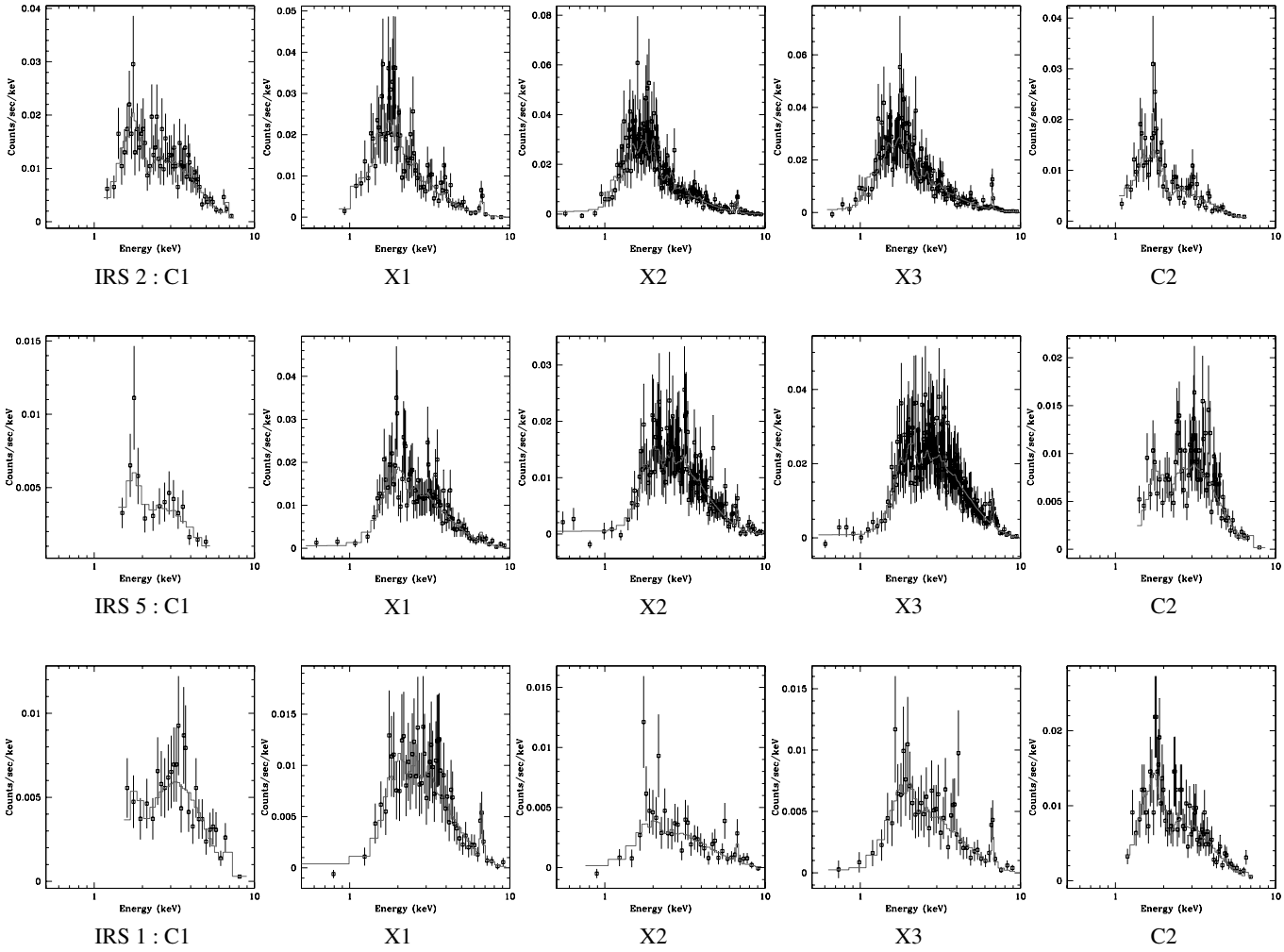

Fig. 5. X-ray spectra of IRS 2, 5 and 1 derived from the five X-ray datasets. The line shows the result of fitting an absorbed APEC model.

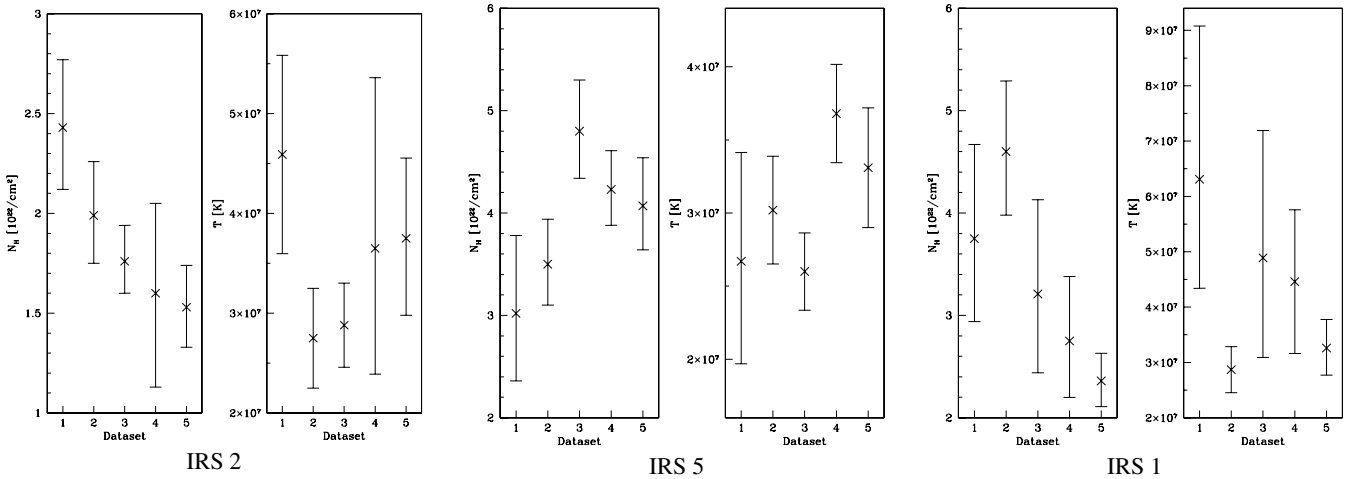

Fig. 6. Results of fitting XSWABS×XSAPEC, fit parameters $N_{\rm H}$ and kT. Abundances set to values determined from best spectra. Errorbars are 3σ. The X-ray datasets are numbered according to Table 2. The NIR-determined $N_{\rm H}$ column densities from Nisini et al. (2005) are 6×10^{22} cm^{-2} (IRS 1), 4×10^{22} cm^{-2} (IRS 2) and 9×10^{22} cm^{-2} (IRS 5).

weak-line T Tauri star. Due to the compact grouping of protostars surrounding it, it remains unclear whether IRS 5 powers an outflow (e.g. Wang et al. 2004). The weak neighbouring radio source (No. 5 in Tables 3 and 4) has a very faint 2MASS counterpart within the nebulosity surrounding IRS 5.

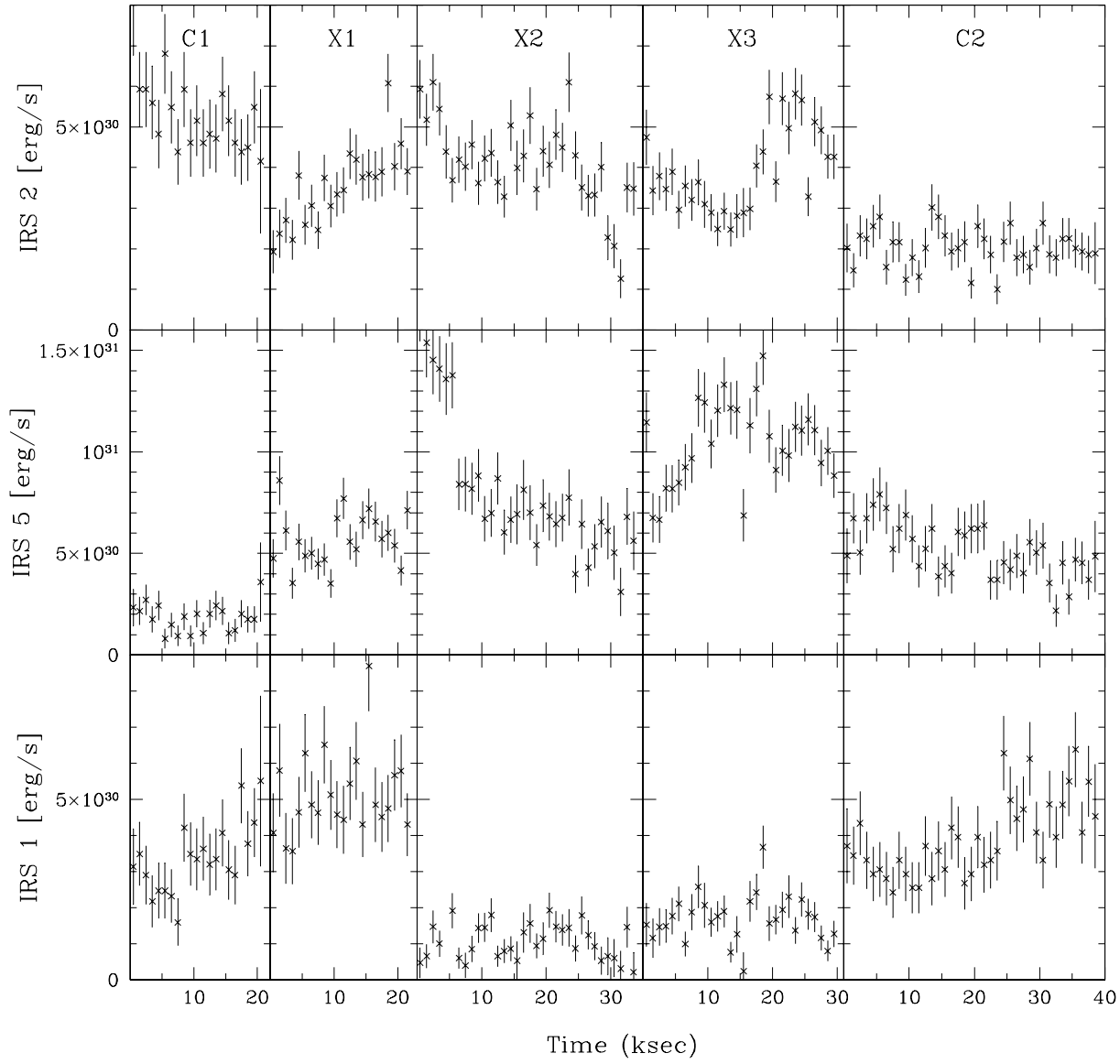

Fig. 7. Kilosecond-binned, background-subtracted X-ray luminosity curves in temporal order for the three class I protostars IRS 2,5, and 1. In the X2 and X3 observations, around 20% of the flux from IRS 1 is lost due to a chip gap in the source region.

IRS 1 was not found to be variable at radio frequencies of 4.9 GHz (Suters et al. 1996). In our data, this source does not show significant radio variability either (Fig. 3 and Table 4). The observed flux is compatible with the value measured by Feigelson et al. (1998). There are, however, clear signs of X-ray variability in this relatively bright X-ray source – within the datasets as well as on longer time scales. The C2 count rate is 35% greater than the C1 count rate, and the XMM-*Newton* count rates also suggest variability even though the X2 and X3 count rates are affected by a chip gap in the source region, which causes a flux loss af about 20%. The X-ray luminosity curves (Fig. 7) show only slight variability within the single observations. The X-ray spectra (Fig. 5) can be modeled by highly absorbed ($N_{\rm H} \approx 3.5\times10^{22}$ cm^{-2}) emission of hot plasma ($T \approx 5\times10^7$ K). There is a significant difference in the absorbing column densities derived from the X1 and C2 observations. No such signs of differences in the fitted plasma temperatures are seen (Fig. 6 and Table 6). According to Wang et al. (2004), IRS 1 could be the powering source of four Herbig-Haro objects. Nisini et al. (2005) find that 80% of this object's bolometric luminosity is due to accretion (see also Nisini et al. 2004, who find evidence for an accelerating wind in the vicinity of IRS 1).

IRS 9 is detected as a weak X-ray source throughout all datasets studied here, shows an X-ray flare in the C1 *Chandra* data (not shown), however, was not detected at radio wavelengths ($S < 0.035$ mJy). This is consistent with previous radio observations.

3.3.2. Radio Source 5 and IRS 6: a candidate brown dwarf and a T Tauri star

Radio Source 5, initially observed by Brown (1987), has not been detected at X-ray wavelengths. In our data, its radio

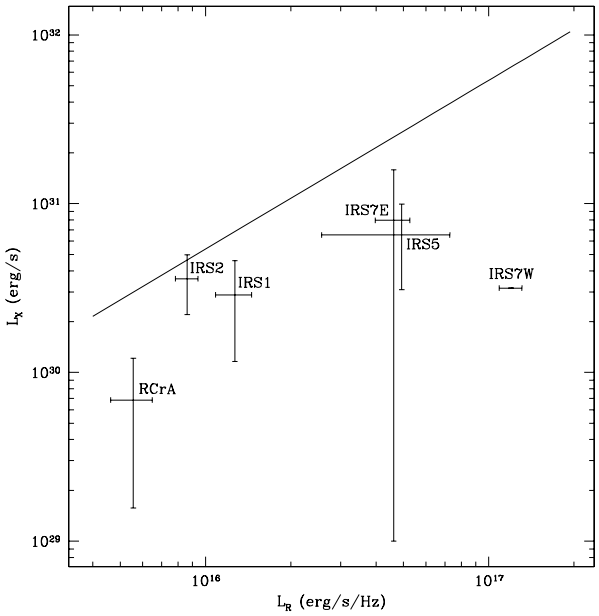

Fig. 8. X-ray vs. radio luminosity of identified young stellar objects for which X-ray luminosities can be derived from spectra. The errorbars correspond to the standard deviation within the 1998 VLA and archival X-ray data, except for IRS 7E/W, where the X-ray luminosities are from Hamaguchi et al. (2005). For IRS 7E, the X-ray errorbars reflect the flare seen in X2/X3 while for IRS 7W, only a single luminosity was determined from the X2 data. The line shows the empirical relationship for active late-type stars from Benz & Guedel (1994).

intensity is variable on timescales of days to months (Fig. 3 and Table 4). Feigelson et al. (1998) report a radio flux on a similar scale. Variability of this source at radio frequencies (4.9 GHz) was also reported by Suters et al. (1996) who argue against an extragalactic origin of the emission. Given its faint infrared counterpart, this source could be a brown dwarf (Wilking et al. 1997; Feigelson et al. 1998). If confirmed, the radio data presented here together with the data analyzed by Suters et al. (1996) would constitute an interesting dataset of long-term variability of brown dwarf radio emission.

IRS 6, detected as a weak X-ray source by *Chandra* as well as XMM-*Newton*, was only found in the combined AM596 *uv*-data: its emission is very weak at 0.15 mJy. No radio emission from this source has been reported before. While this source is too weak for an analysis of short-timescale X-ray variability, the emission is somewhat weaker in the 2003 (C2) data when compared to the 2000 (C1) level. The X2 and X3 count rates for IRS 6 are affected by a chip gap in the source region. Wang et al. (2004), looking for optical outflows, argue that IRS 6 could be the driving source of four Herbig-Haro objects. Nisini et al. (2005) resolve this source into a binary object with a separation of only 112 AU (scaled to d = 150 pc), making the attribution of X-rays difficult. However, they find no sign of ongoing accretion in the near-infrared towards IRS 6a. Thus, IRS 6 appears to contain at least one T Tauri star.

3.3.3. The IRS 7 complex with its two deeply embedded protostars

Two main sources can be detected in the IRS 7 region, at both radio and X-ray wavelengths, namely IRS 7E and IRS 7W. Another major radio source is located five arcseconds north of IRS 7W (Radio Source 9, as defined by Brown 1987). Three additional weak radio sources accompany IRS 7E/W.

There has been confusion about possible protostellar sources detected at different wavelengths around IRS 7, although some clarification was brought by Nutter et al. (2005), presenting submillimeter data where the single emission peak observed before at millimeter wavelengths (Henning et al. 1994; Chini et al. 2003; Groppi et al. 2004) is resolved into three subsources. A molecular outflow and a disk were detected in the IRS 7 region and analyzed by Anderson et al. (1997) and Groppi et al. (2004), although the latter showed that it is not yet possible to attribute these to any of the sources seen at higher angular resolution. IRS 7 is also the driving source of Herbig-Haro objects (Wang et al. 2004). Harju et al. (2001) find evidence for a jet emanating from IRS 7E at λ = 6 cm, using the ATCA radio interferometer. Choi & Tatematsu (2004) analyze the IRS 7 region at λ = 6.9 mm with the VLA. Interestingly, they only marginally detect IRS 7E while there is elongated emission around IRS 7W and Radio Source 9, although the connection remains unclear. The emerging picture is that of IRS 7W being an infrared-detected, deeply embedded protostar, probably a class I or II source, while IRS 7E could be a class 0 source although the source was detected at 4.8 μm by Pontoppidan et al. (2003). This would be one of the first class 0 sources detected in X-rays.

IRS 7E is quite variable on all timescales covered in the 1998 VLA data (Fig. 3 and Table 4), at a flux level mostly below the value reported by Feigelson et al. (1998). The weak radio source detected in the eastern vicinity of IRS 7E (source 15) might be a sign for extended radio emission. The radio sources detected around IRS 7E/W are shown in an inset of Fig. 2.

IRS 7E is the most variable X-ray source among the objects studied here. While IRS 7E was only marginally detected in the C1, X1, and C2 observations, the 2003 (X2, X3) datasets show IRS 7E as a strong and very hard X-ray source. This flaring has been studied by Hamaguchi et al. (2005) who argue that this might be an X-ray detected class 0 source. They do not find any near-infrared counterpart down to a K-band magnitude of 19. However, Pontoppidan et al. (2003) detect both sources, IRS 7E/W, at 4.8 μm using VLT-ISAAC, arguing that IRS 7E remained undetected at 10 μm (Wilking et al. 1997) due to silicate absorption. It is tempting to attribute also the enormous flare observed by Koyama et al. (1996) to this source, although that remains unclear due to the limited angular resolution of their ASCA data. Since spectra of IRS 7E could only be taken from the XMM-*Newton* data, an estimated luminosity curve for this source was produced by assuming the same spectral characteristics, taken from Hamaguchi et al. (2005), of kT = 3 keV (corresponding to a temperature of ≈35 MK, rather a lower limit) and $N_{\rm H} = 2.8 \times 10^{23}$ cm^{-2} for all five datasets, then determining the fluxes and luminosities following the procedure outlined above. To minimize contamination,

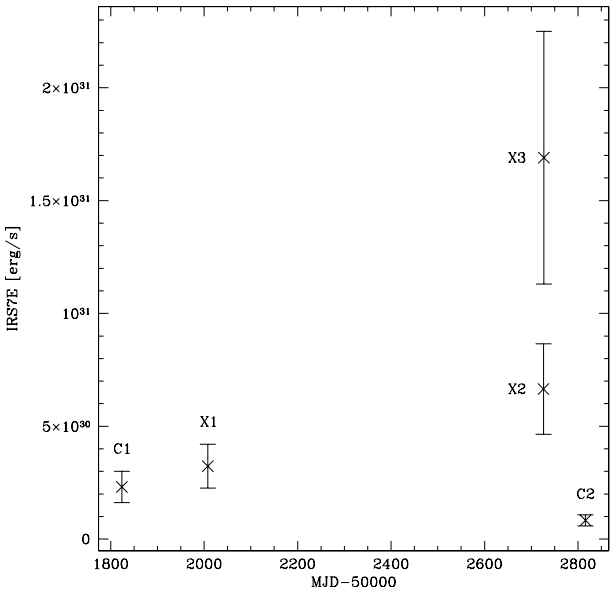

Fig. 9. IRS 7E X-ray luminosity. Countrates for the five X-ray datasets were converted into luminosities without background subtraction, assuming a single-temperature spectrum of $kT = 3$ keV and $N_{\rm H} = 2.8 \times 10^{23}$ cm^{-2} (Hamaguchi et al. 2005). The errorbars denote errors of 30%. Note that the source is only marginally detected in C1 and C2.

Hamaguchi et al. (2005) excluded IRS 7W from the IRS 7E source region in their analysis. The plot shows the enormous increase in luminosity (Fig. 9). In the two *Chandra* observations, only 19 and 13 – however highly energetic – photons were recorded from IRS 7E respectively. Given the high temperature of the plasma emission as well as the quick variability, especially when comparing the subsequent X2 and X3 datasets, it appears unlikely that the emission is due to an accretion shock. These characteristics rather point towards circumstellar magnetic activity.

IRS 7W is the brightest radio source in the sample considered here, mostly emitting at around 4.2 mJy, although in two epochs the source is detected at >5 mJy (Fig. 3 and Table 4). This source shows only moderate radio variability within the 1998 monitoring, especially on timescales of days. For Radio Source 9, Feigelson et al. (1998) report an 8.4 GHz flux density of 1.58 mJy, considerably higher than all fluxes measured in 1998 which are <1.1 mJy. Close to Radio Source 9, there are two weak radio sources (sources 10 and 13) which do not have counterparts at other wavelengths.

In the C1/C2 data, IRS 7W is detected as a weak X-ray source emitting energetic photons, similar to IRS 7E. Due to contamination caused by the flaring nearby source IRS 7E, a meaningful spectrum could only be extracted from the X2 dataset, leading to $kT = 4.7$ keV (≈55 MK) and $N_{\rm H} = 3.4 \times 10^{23}$ cm^{-2} (Hamaguchi et al. 2005).

3.3.4. The Herbig Ae star R CrA

R CrA is one of the optically brightest ($V \sim 11.5$ mag) objects in the CrA cloud and it illuminates the reflection nebulosity NGC 6729. The stellar parameters are somewhat uncertain, especially because the optical spectrum seems to be variable and spectral types ranging from B8 to F7 have been reported (e.g. Bibo et al. 1992). Here we adopt the values listed in Lorenzetti et al. (1999), i.e. spectral type A5e, $L_{\rm bol} = 132\,L_\odot$, and $A_{\rm V} = 1.9$ mag. Comparison of these parameters to the pre-main sequence models of Palla & Stahler (1999) suggest a mass of ∼3.5 $M_\odot$ and an age of slightly more than 1 Myr for R CrA.

The spectral energy distribution of R CrA rises very steeply between 0.6 μm and 3 μm (see, e.g. Acke & van den Ancker 2004), demonstrating the presence of large amounts of hot circumstellar material, presumably in the form of an optically thick circumstellar disk. This very large infrared excess suggests that R CrA is in a very early evolutionary state and thus we discuss it here together with the lower-mass protostars.

In the VLA data (Fig. 3 and Table 4), R CrA was detected as a weak and rather constant radio source with an average flux of 0.23 mJy, the same flux level as measured by Feigelson et al. (1998). However, R CrA remained undetected at radio wavelengths several times before: in September 1985 (VLA, 6 cm, $3\sigma = 0.17$ mJy, Brown 1987), in February 1990 (VLA, 3.6 cm, $3\sigma = 0.10$ mJy, Skinner et al. 1993) as well as with the VLA and the AT in 1985–87 and 1992, respectively (Suters et al. 1996). Even though R CrA is quite close to the respective 5σ limits, this is suggestive of long-term variability.

X-ray observations of the *Coronet* region with EINSTEIN and ROSAT did not detect X-ray emission from R CrA (Zinnecker & Preibisch 1994; Damiani et al. 1994; Neuhäuser & Preibisch 1997; Walter et al. 1997). Koyama et al. (1996) detected hard X-ray emission near the location of R CrA with ASCA. However, due to the poor spatial resolution of the ASCA data (*FWHM* ∼ 2′) the contributions of the individual young stellar objects R CrA, IRS 7, and IRS 9 could not be resolved. Nevertheless, since the intensity peak in the ASCA image was located close to the position of R CrA, it appears likely that R CrA produced a significant fraction of the observed hard X-ray emission. During this ASCA observation a strong flare was seen. The X-ray spectrum was found to be very hard and could be fitted with a $kT \sim 6$–7 keV plasma model and an absorbing hydrogen column density of $N_{\rm H} \sim 4 \times 10^{22}$ cm^{-2}. During the flare, the spectrum showed a remarkable broadened or double emission line structure between 6.2 and 6.8 keV. However, it remained unclear which of the sources caused the flare.

X-ray emission from R CrA is clearly detected in all the *Chandra* and XMM-*Newton* data sets used in this paper. The detection in the *Chandra* observation C1 was already noted by Skinner et al. (2004). During both *Chandra* observations R CrA is only seen as a rather weak source, yielding no more than ∼100 counts, too few for detailed spectral analysis. During the first XMM-*Newton* observation the observed count rate for R CrA is well consistent with that in the *Chandra* observations, but during the XMM-*Newton* observations X2 and X3 the count rates were about a factor of two larger (see lightcurve in Fig. 11). The lightcurves show no indications of a flare, it appears rather as if the source has "switched" to a higher activity level duringX2 and X3. A sudden drop of the count rate (by about a factor of two) is seen in the second half of observation X3. A possible interpretation for the general shape of the

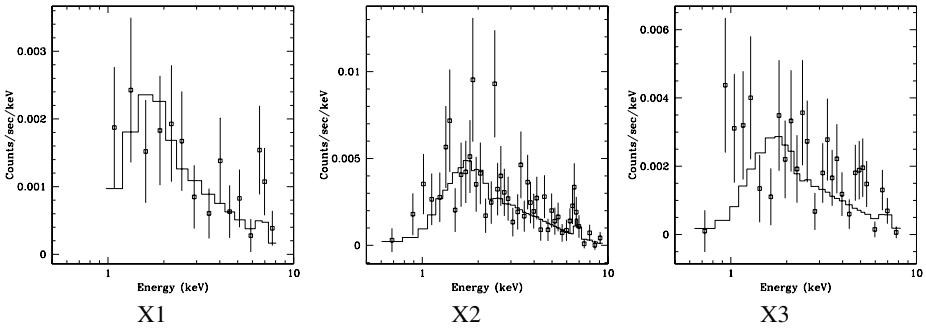

Fig. 10. R CrA spectra, taken from an ellipse region avoiding the neighbouring source IRS 9. The results of fitting an absorbed APEC model are shown. In the X3 fit, the column density was frozen to the values from X1 and X2.

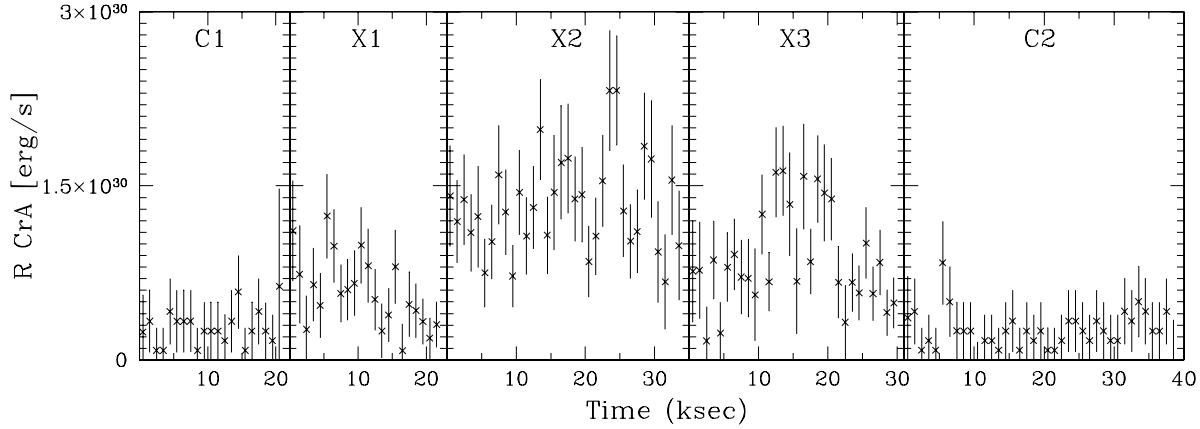

Fig. 11. R CrA X-ray luminosity curves from the same elliptical region also used for the spectra. Luminosity calculated assuming spectral properties of the best spectrum (X2). Data is kilosecond-binned and background-subtracted, datasets are in temporal order as labeled.

lightcurve would be the temporal presence of a dominant active region during X2 and X3. The sharp drop in X3 may then be explained by the occultation of such an active region when the stellar rotation moves it behind the stellar disk.

The X-ray spectra of R CrA extracted from observations X1, X2, and X3 show a very strong high-energy tail and a pronounced 6.7 keV emission line, providing clear evidence for very hot plasma. The spectral fits yield a plasma temperature of about 100 MK, the highest value of all sources in the *Coronet* region. The hydrogen column densities derived from the spectral fits are $\sim 1.3 \times 10^{22}$ cm^{-2} and correspond to an optical extinction of $A_{\mathrm{V,X}} \sim 6{-}8$ mag (Ryter 1996; Vuong et al. 2003). This is higher than the extinction estimate derived from the optical properties ($A_{\mathrm{V}} \sim 2$ mag), but given the uncertainty of the optical parameters of R CrA, both values may well be in agreement.

The X-ray luminosity of R CrA derived from the spectral fits ranges from 2.5×10^{29} erg/s in the C2 observation to 1.3×10^{30} erg/s in the X2 observation. The fractional X-ray luminosity is thus $\log(L_{\mathrm{X}}/L_{\mathrm{bol}}) \sim -6.3 \ldots - 5.6$.

The observed X-ray emission of R CrA is particularly interesting since, according to our current understanding of stellar X-ray emission mechanisms, one would not expect to see any X-ray emission emission from this star. Being an intermediate-mass A-type star, R CrA should neither possess a magnetically driven corona, which is the source of the X-ray emission from late type (F to M) stars, nor can it have a strong radiation driven stellar wind, in which shocks cause X-ray emission observed in the more massive O- and early B-type stars (see e.g. Pallavicini 1989; Favata & Micela 2003). The theoretical expectation that late B and A stars should not be instrinsic X-ray emitters is well confirmed in the case of main sequence stars (e.g. Schmitt et al. 1993; Cassinelli et al. 1994). However, it is still unclear whether the Herbig Ae/Be stars, i.e. the class of very young intermediate-mass pre-main sequence stars, to which R CrA belongs, also fit to this scenario. In EINSTEIN, ROSAT, ASCA, and *Chandra* X-ray observations of samples of Herbig Ae/Be stars (Damiani et al. 1994; Zinnecker & Preibisch 1994; Preibisch & Zinnecker 1996; Skinner et al. 2004; Hamaguchi et al. 2005) some 30–50% of the observed stars were detected as X-ray sources. Several possible explanations have been proposed for these findings (see Caillault et al. 1994; Preibisch & Zinnecker 1996; Skinner et al. 2004), but no final explanation has been found. There exist some ideas how an AeBe star may produce X-ray emission (e.g. the scenario of a nonsolar dynamo powered by rotational shear in very young intermediate mass stars; see Tout & Pringle 1995), but no really convincing evidence has yet been found for this. A possible explanation for the observed X-ray emission may be that the X-rays originate not from the AeBe stars themselves, but from close, unresolved, late type companions.

For our case of R CrA, we note that Takami et al. (2003) presented spectro-astrometric observations and found some evidence for the presence of a companion at a separation of about

$\sim$0.070″–0.10″, i.e. only 10–15 AU. If such a companion actually exists, it is probably a lower-mass young stellar object, i.e. a T Tauri star or a low-mass protostar, which could easily explain the observed X-ray emission.

What remains quite remarkable, however, is the extremely high plasma temperature of $\sim$100 MK inferred from the X-ray spectra. Typical plasma temperatures in young stellar objects range from $\sim$10 MK up to $\sim$50 MK, reaching higher values usually only during large X-ray flares[5]. From other X-ray observations of star forming regions it seems that class I protostars show systematically higher plasma temperatures than the more evolved T Tauri stars (see, e.g., Imanishi et al. 2001, for the case of ρ Oph). This may be an indication that the companion of R CrA is a very young object (i.e. more likely a class I protostar than a T Tauri star). In this case, some (perhaps the largest) fraction of the infrared excess emission may come from the companion and not from the Ae star R CrA itself.

4. Conclusions and outlook

We presented the results of radio monitoring of protostars in the *Coronet* cluster together with archival X-ray data of these sources covering 154 ks. The main results are:

1. Observing with the VLA in nine epochs spread over several months in 1998, we detect centimetric radio emission from 13 sources in the region around R CrA. Nine sources in this region are detected in X-rays, and eight sources are detected at both radio and X-ray wavelengths.
2. IRS 5, a class I protostar with nonthermal radio emission, shows an interesting increase and decrease in its radio emission on the order of days, accompanied by changes in its polarization properties. It is the most variable radio source in the 1998 VLA data. Among the three protostars bright enough for a detailed X-ray study, IRS 5 is also the most variable source in X-rays.
3. Not counting IRS 7W due to the unclear classification, we detect three out of four covered class I sources in radio emission, while we detect all four in X-rays. With IRS 7E, one candidate class 0 source is detected in X-rays as well as in radio emission.
4. The Herbig Ae star R CrA was detected at both radio and X-ray wavelengths. The X-ray spectrum of this source surprisingly contains emission from extremely hot plasma ($\approx$100 MK). We suspect that a lower-mass companion is responsible for this emission.
5. The spectra of IRS 1, 2 and 5 all can be explained by the absorbed emission of plasma having temperatures of several 10^7 K while the high absorbing column densities (several 10^{22} cm^{-2}) are all at about half the values determined from near-infrared colours. While this has been observed before towards similar sources, the effect remains unexplained. We discuss possible explanations.
6. While the X-ray lightcurves of the the class I protostars IRS 1, 2, and 5 all show varying degrees of variability, no flare events were observed. With no class II sources to compare with, it is impossible here to corroborate the conclusion of Imanishi et al. (2001) that class I sources are intrinsically more X-ray–variable than later evolutionary stages, although the three class I sources studied here are not extremely variable.
7. The X-ray spectra are spread over about 2.5 years and also allow for an analysis of variability in their main fit parameters, absorbing column density and plasma temperature. While mostly no significant variability can be seen, a significant change is observed in the absorbing column density towards IRS 2: It appears to have decreased continuously to a significantly lower level, from 2.4×10^{22} cm^{-2} to 1.5×10^{22} cm^{-2}, possibly due to a clumpy circumstellar medium towards this source.

Studying the *Coronet* cluster at radio and X-ray wavelengths has provided a number of interesting insights. In order to learn more about high-energy processes in these young stellar objects, we plan to carry out simultaneous X-ray, radio, and near-infrared observations of the *Coronet* cluster in August 2005 with *Chandra*, the VLA and at ESO.

Acknowledgements. The National Radio Astronomy Observatory is a facility of the National Science Foundation operated under cooperative agreement by Associated Universities, Inc. This study is partly based on observations obtained with XMM-*Newton*, an ESA science mission with instruments and contributions directly funded by ESA Member States and NASA.

[5] In the most comprehensive data set on the X-ray emission from young stars, the Chandra Orion Ultradeep Project, only 2% of the optically visible T Tauri stars in the Orion Nebula Cluster showed plasma temperatures exceeding 100 MK (see Getman et al. 2005; Preibisch et al. 2005).

References

Acke, B., & van den Ancker, M. E. 2004, A&A, 426, 151
Anderson, I. M., Harju, J., Knee, L. B. G., & Haikala, L. K. 1997, A&A, 321, 575
André, P. 1996, in Radio Emission from the Stars and the Sun, ed. A. R. Taylor, & J. M. Paredes, ASP Conf. Ser., 93, 273
André, P., Montmerle, T., Feigelson, E. D., Stine, P. C., & Klein, K.-L. 1988, ApJ, 335, 940
André, P., Deeney, B. D., Phillips, R. B., & Lestrade, J. 1992, ApJ, 401, 667
André, P., Ward-Thompson, D., & Barsony, M. 2000, in Protostars and Planets IV, ed. V. Mannings, A. P. Boss, & S. S. Russell, 59
Bally, J., Feigelson, E., & Reipurth, B. 2003, ApJ, 584, 843
Benz, A. O., & Guedel, M. 1994, A&A, 285, 621
Bibo, E. A., The, P. S., & Dawanas, D. N. 1992, A&A, 260, 293
Birk, G. T., Schwab, D., Wiechen, H., & Lesch, H. 2000, A&A, 358, 1027
Bower, G. C., Plambeck, R. L., Bolatto, A., et al. 2003, ApJ, 598, 1140
Brown, A. 1987, ApJ, 322, L31
Caillault, J., Gagne, M., & Stauffer, J. R. 1994, ApJ, 432, 386
Carkner, L., Kozak, J. A., & Feigelson, E. D. 1998, AJ, 116, 1933
Cassinelli, J. P., Cohen, D. H., Macfarlane, J. J., Sanders, W. T., & Welsh, B. Y. 1994, ApJ, 421, 705
Chen, W. P., & Graham, J. A. 1993, ApJ, 409, 319
Chini, R., Kämpgen, K., Reipurth, B., et al. 2003, A&A, 409, 235
Choi, M., & Tatematsu, K. 2004, ApJ, 600, L55
Damiani, F., Micela, G., Sciortino, S., & Harnden, F. R. 1994, ApJ, 436, 807

Favata, F., & Micela, G. 2003, Space Sci. Rev., 108, 577
Favata, F., Flaccomio, E., Reale, F., et al. 2005, ApJS, in press
Feigelson, E. D., & Montmerle, T. 1999, ARA&A, 37, 363
Feigelson, E. D., Welty, A. D., Imhoff, C., et al. 1994, ApJ, 432, 373
Feigelson, E. D., Carkner, L., & Wilking, B. A. 1998, ApJ, 494, L215
Feigelson, E. D., Broos, P., Gaffney, J. A., et al. 2002, ApJ, 574, 258
Feigelson, E. D., Gaffney, J. A., Garmire, G., Hillenbrand, L. A., & Townsley, L. 2003, ApJ, 584, 911
Finkenzeller, U., & Mundt, R. 1984, A&AS, 55, 109
Fleming, T. A., Schmitt, J. H. M. M., & Giampapa, M. S. 1995, ApJ, 450, 401
Gagné, M., Skinner, S. L., & Daniel, K. J. 2004, ApJ, 613, 393
Garmire, G., Feigelson, E. D., Broos, P., et al. 2000, AJ, 120, 1426
Garmire, G. P., & Garmire, A. B. 2003, Astron. Nachr., 324, 153
Getman, K. V., Flaccomio, E., Broos, P. S., et al. 2005, ApJ, in press
Gibb, A. G. 1999, MNRAS, 304, 1
Groppi, C. E., Kulesa, C., Walker, C., & Martin, C. L. 2004, ApJ, 612, 946
Grosso, N., Montmerle, T., Feigelson, E. D., et al. 1997, Nature, 387, 56
Güdel, M. 2002, ARA&A, 40, 217
Güdel, M. 2004, A&ARv, 12, 71
Guenther, E. W., Stelzer, B., Neuhäuser, R., et al. 2000, A&A, 357, 206
Hamaguchi, K., Corcoran, M. F., Petre, R., et al. 2005, ApJ, 623, 291
Harju, J., Higdon, J. L., Lehtinen, K., & Juvela, M. 2001, in Science with the Atacama Large Millimeter Array, ed. A. Wootten, ASP Conf. Ser., 235, 125
Hayashi, M. R., Shibata, K., & Matsumoto, R. 1996, ApJ, 468, L37
Henning, Th., Launhardt, R., Steinacker, J., & Thamm, E. 1994, A&A, 291, 546
Hodapp, K. 1994, ApJS, 94, 615
Imanishi, K., Koyama, K., & Tsuboi, Y. 2001, ApJ, 557, 747
Isobe, H., Shibata, K., Yokoyama, T., & Imanishi, K. 2003, PASJ, 55, 967
Knude, J., & Høg, E. 1998, A&A, 338, 897
Koyama, K., Hamaguchi, K., Ueno, S., Kobayashi, N., & Feigelson, E. D. 1996, PASJ, 48, L87
Lada, C. J. 1987, in Star Forming Regions, ed. M. Peimbert, & J. Jugaku, IAU Symp., 115, 1
Lehtinen, K., Harju, J., Kontinen, S., & Higdon, J. L. 2003, A&A, 401, 1017
Lorenzetti, D., Tommasi, E., Giannini, T., et al. 1999, A&A, 346, 604
Lucas, P. W., Blundell, K. M., & Roche, P. F. 2000, MNRAS, 318, 526
Marraco, H. G., & Rydgren, A. E. 1981, AJ, 86, 62
Montmerle, T. 2003, Adv. Space Res., 32, 1067
Montmerle, T., Grosso, N., Tsuboi, Y., & Koyama, K. 2000, ApJ, 532, 1097
Mukai, K. 1993, Legacy, 3, 21
Neuhäuser, R. 1997, Science, 276, 1363
Neuhäuser, R., & Preibisch, T. 1997, A&A, 322, L37
Neuhäuser, R., Walter, F. M., Covino, E., et al. 2000, A&AS, 146, 323
Nisini, B., Antoniucci, S., & Giannini, T. 2004, A&A, 421, 187
Nisini, B., Antoniucci, S., Giannini, T., & Lorenzetti, D. 2005, A&A, 429, 543
Nutter, D. J., Ward-Thompson, D., & André, P. 2005, MNRAS, 357, 975
Ozawa, H., Grosso, N., & Montmerle, T. 2005, A&A, 429, 963
Palla, F., & Stahler, S. W. 1999, ApJ, 525, 772
Pallavicini, R. 1989, A&AR, 1, 177
Phillips, R. B., Lonsdale, C. J., & Feigelson, E. D. 1993, ApJ, 403, L43
Pontoppidan, K. M., Fraser, H. J., Dartois, E., et al. 2003, A&A, 408, 981
Preibisch, T. 2003a, A&A, 410, 951
Preibisch, T. 2003b, A&A, 401, 543
Preibisch, T. 2004a, Ap&SS, 292, 631
Preibisch, T. 2004b, A&A, 428, 569
Preibisch, T., & Zinnecker, H. 1996, in MPE Report 263, Roentgenstrahlung from the Universe, ed. H. U. Zimmermann, J. Trümper, & H.W. Yorke, 17
Preibisch, T., & Zinnecker, H. 2001, AJ, 122, 866
Preibisch, T., & Zinnecker, H. 2002, AJ, 123, 1613
Preibisch, T., Kim, Y.-C., Favata, F., et al. 2005, ApJS, in press
Rieke, G. H., & Lebofsky, M. J. 1985, ApJ, 288, 618
Rodríguez, L. F., Anglada, G., & Curiel, S. 1999, ApJS, 125, 427
Ryter, C. E. 1996, Ap&SS, 236, 285
Schmitt, J. H. M. M., Zinnecker, H., Cruddace, R., & Harnden, F. R. 1993, ApJ, 402, L13
Shang, H., Lizano, S., Glassgold, A., & Shu, F. 2004, ApJ, 612, L69
Shu, F. H., Shang, H., Glassgold, A. E., & Lee, T. 1997, Science, 277, 1475
Skinner, S. L. 1993, ApJ, 408, 660
Skinner, S. L., Brown, A., & Stewart, R. T. 1993, ApJS, 87, 217
Skinner, S. L., Güdel, M., Audard, M., & Smith, K. 2004, ApJ, 614, 221
Smith, K., Güdel, M., & Benz, A. O. 1999, A&A, 349, 475
Suters, M., Stewart, R. T., Brown, A., & Zealey, W. 1996, AJ, 111, 320
Takami, M., Bailey, J., & Chrysostomou, A. 2003, A&A, 397, 675
Taylor, K. N. R., & Storey, J. W. V. 1984, MNRAS, 209, 5P
Tout, C. A., & Pringle, J. E. 1995, MNRAS, 272, 528
Tsuboi, Y., Koyama, K., Hamaguchi, K., et al. 2001, ApJ, 554, 734
Tsujimoto, M., Koyama, K., Kobayashi, N., et al. 2004, PASJ, 56, 341
Vuong, M. H., Montmerle, T., Grosso, N., et al. 2003, A&A, 408, 581
Walter, F. M., Vrba, F. J., Wolk, S. J., Mathieu, R. D., & Neuhäuser, R. 1997, AJ, 114, 1544
Wang, H., Mundt, R., Henning, T., & Apai, D. 2004, ApJ, 617, 1191
White, S. M., Pallavicini, R., & Kundu, M. R. 1992, A&A, 259, 149
Wilking, B. A., Greene, T. P., Lada, C. J., Meyer, M. R., & Young, E. T. 1992, ApJ, 397, 520
Wilking, B. A., McCaughrean, M. J., Burton, M. G., et al. 1997, AJ, 114, 2029
Wilking, B. A., Taylor, K. N. R., & Storey, J. W. V. 1986, AJ, 92, 103
Zinnecker, H., & Preibisch, T. 1994, A&A, 292, 152